ChemComm

COMMUNICATION

Gold-loaded nanoporous superparamagnetic nanocubes for catalytic signal amplification in detecting miRNA†

Received 00th January 20xx,
Accepted 00th January 20xx

DOI: 10.1039/x0xx00000x

www.rsc.org/

Mostafa Kamal Masud,[a,b] Md. Nazmul Islam,[b,c] Md. Hakimul Haque,[c,d] Shunsuke Tanaka,[a] Vinod Gopalan,[d] Gursel Alici,[e] Nam-Trung Nguyen,[b] Alfred King-yin Lam,[d] Md. Shahriar A. Hossain,*[a] Yusuke Yamauchi*[a] and Muhammad J. A. Shiddiky*[b,c]

This paper reports the development of a nonenzymatic, amplification-free, and sensitive platform for the detection of microRNA based on a new class of electrocatalytically acative superparamagnetic gold-loaded nanoporous iron oxide nanocubes (Au@NPFe$_2$O$_3$NC). The assay showed an excellent detection sensitivity down to 100 fM and specificity towards the analysis of miR-21 in cell lines and tissue samples derived from patients with esophageal squamous-cell carcinoma (ESCC).

Nanostructured magnetic nanoparticles (NPs) have attracted an immense interest for a broad range of applications in the areas of catalysis, nanotechnology and biotechnology.[1] They have unique magnetic characteristics (e.g., superparamagnetism, high values of saturation magnetization, easy control by small magnetic fields), biochemical characteristics (e.g., nontoxicity, biodegradability, biocompatibility), intrinsic enzyme mimicking activity, low cost of synthesis, and ability to catalyse redox reaction of various organic and inorganic compounds.[2] Introducing pores into the NPs offer a high surface area relative to volume that make it highly capable for uptaking and releasing biological guest molecules.[3] This porous metal structure possesses enhanced catalytic capacity as they maximise surface dependent mass transport as compared to that of bulk materials of the same mass. In addition, porous NPs offer several advantages in catalysis including stabilization of particles from sintering, an expedition of cascade reaction by placing catalytic functionality in sequential compartments, and enhancement of the selectivity of catalysis by molecular sieving. Composite nanomaterials also attract increasing attention because of their combined physicochemical properties and potential for catalysis and biosensing applications.[4] They have more superior characteristics than the monometallic frameworks counterparts. For instance, iron oxides (Fe_3O_4 or γ-Fe_2O_3) containing gold nanoparticle (AuNPs) exhibits combined advantages and serendipitous properties of both Fe_3O_4 and AuNPs.[5] The combination of high surface area, conductivity, thermal/chemical stability and superparamagnetism of Fe_2O_3 with bio-favourable physicochemical properties of AuNPs (*i.e.* affinity interaction of DNA/RNA with gold) makes gold-loaded nanoporous Fe_2O_3 nanocubes (Au@NPFe$_2$O$_3$NC) extremely suitable for developing biosensors for a wide range for molecular biomarkers including micro RNA (miRNA).

miRNAs are small non-coding RNAs with 21-24 nucleotides which can regulate gene expressions by modulating its downstream proteins. Recent studies have also confirmed the use of miRNAs as biomarkers for diagnosis and prognosis of many diseases including cancer.[6] Over the past decades, many conventional approaches such as northern blotting, microarrays, in-situ hybradisation and quantitative real-time PCR (qRT-PCR) have been used for the analysis of miRNA. Each of these methods has their own advantages and disadvantages. For examples, qRT-PCR can give a quantification of miRNA but has a very low throughput. Additionally, most of these methods use PCR amplification, which are still affected by amplification bias, fluorescent labelling and rely on complicated and expensive protocols.[7] As an alternative to these methods, a large number of biosensors have been developed based on hybridization, oligonucleotides labelled with enzymes and redox indicator.[8] Despite the superior analytical performance, these sensors often involve complex and tedious amplification processes, expensive biomaterials, time-consuming and laborious procedures.[9] Therefore, development of a simple, inexpensive and rapid miRNA biosensor would be highly beneficial for miRNA-based molecular diagnositics of patients with chronic diseases. In this study, we synthesed and characterized a new class of Au@NPFe$_2$O$_3$NC. The

[a] Institute for Superconducting and Electronic Materials, Australian Institute for Innovative Materials (AIIM), University of Wollongong, Innovation Campus, North Wollongong, NSW 2519, Australia
[b] Queensland Micro- and Nanotechnology Centre (QMNC), Griffith University, Nathan, QLD 4111, Australia
[c] School of Natural Sciences, Griffith University, Nathan, QLD 4111, Australia
[d] Cancer Molecular Pathology laboratory in Menzies Health Institute Queensland, Griffith University and School of Medicine, Gold Coast, Australia
[e] ARC Centre of Excellence for Electromaterials Science, University of Wollongong, Northfields Avenue, Wollongong, NSW 2522, Australia

† Electronic Supplementary Information (ESI) available: Detailed experimental section and table, and supplementary figures. See DOI: 10.1039/x0xx00000x

electrocatalytic activity of this nanocube was used to develop a miRNA biosensor. The sensor was tested in cell lines and tissue samples obtained from patients with oesophageal squamous cell carcinoma (ESSC).

Au@NPFe$_2$O$_3$NC was synthesized by deposition of AuNPs on the nanoporous iron oxide nanocubes (NPFe$_2$O$_3$NCs) derived from Prussian blue (PB) nanocubes. Detailed synthetic procedures and characterization are described in the in the ESI†. SEM images of the original PB nanocubes and NPFe$_2$O$_3$NC, wide-angle XRD patterns for original PB nanocubes and Au@NPFe$_2$O$_3$NC, and magnetization curve for Au@NPFe$_2$O$_3$NC was measured at 300 K are shown in Figs. S1-S2, ESI†. After deposition of AuNPs, uniformly sized AuNPs (≈3-6 nm) are distributed on the surface of NPFe$_2$O$_3$NC (Fig. 1A). The loading amount of AuNPs is around 2 wt% in the product (Fig. 1B). The XRD pattern shows the diffraction peaks derived from Au, α-Fe$_2$O$_3$, and γ-Fe$_2$O$_3$ (Fig. S1D). The nanocube is found to be superparamagnetic from the complete reversibility of the *M-H* curve recorded at room temperature (300 K). The S-shaped hysteresis loop is shown in Fig. S2 with the negligible coercive field (H_c) are a typical characteristic of superparamagnetic nanoparticles. The saturation magnetisation (M_s) reported in this study is 16 emu g^{-1} at 300 K for Au@NPFe$_2$O$_3$NC. Due to this sufficient M_s value, the samples can be easily collected by a neodymium magnet. With the loading amount of Au nanoparticles, the M_s value is decreased because of the non-magnetic property of Au.

To assess the electrocatalytic activity of Au@NPFe$_2$O$_3$NC, the Au@NPFe$_2$O$_3$NC-modified glassy carbon electrode (GCE) (see ESI† for detailed fabrication steps) was used as working electrode. The cyclic voltammetric (CV) measurements were carried out in the presence of Ru(NH$_3$)$_6$Cl$_3$ (RuHex), a redox label widely used in electrochemical biosensing.[10] Well-defined cathodic (E_{pc}) and anodic (E_{pa}) peaks for the [Ru(NH$_3$)$_6$]$^{3+/2+}$sytem were obtained at -225 mV and -165 mV (vs Ag/AgCl) at the unmodified GCE (GCE/bare), indicating one-electron reversible process (ΔE = 60 mV, Fig 2A). The Au@NPFe$_2$O$_3$NC-modified GCE (GCE/Au@NPFe$_2$O$_3$NC) offered significantly enhanced cathodic (i_{pc}), and anodic (i_{pa}) peak currents compared to that of the GCE/bare electrode (Fig 2B). Notably, i_{pc} increased approximately four-times (4.6 vs 20.1 μAcm^{-2}) with E_{pc} shifted by ~ -55 mV, whereas i_{pa} increased approximately two-times (2.3 vs 5.2 μAcm^{-2}) with E_{pa} shifted by ~ -30 mV. These data indicate that Au@NPFe$_2$O$_3$NC catalysed both the oxidation and reduction of RuHex, while the rate of the reduction of RuHex is greater than that of the oxidation process. The effect of the pH and temperature of the electrolyte for the electrocatalytic activity of Au@NPFe$_2$O$_3$NC was also studied. An enhanced catalytic response was found in acidic pH and at higher temperature (Figs. S3 and S4 in ESI†). However, due to the physiological conditions, pH 7.0 and room temperature (~25°C) were selected as optimal conditions for all subsequent experiments. To examine the charge transport mechanism, we recorded CVs of both GCE/bare and GCE/Au@NPFe$_2$O$_3$NC as a function of scan rates (10 – 1500 mVs^{-1}). As shown in Fig S5A (ESI†), the currents i_{pc} and i_{pa} increase with increasing scan rate from 10 to 1500 mVs^{-1}, indicating that the Au@NPFe$_2$O$_3$NC

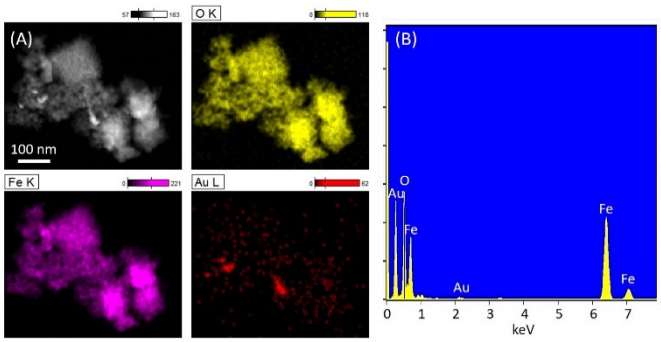

Fig. 1. (A) Elemental mapping images (O, Fe, and Au), and (B) EDX spectrum of Au@NPFe$_2$O$_3$NC.

retained its electrocatalytic activity within the studied scan rates. Fig S5B shows a linear relationship between i_{pc} and i_{pa} with the square root of the scan rate ($v^{1/2}$) for both the unmodified and Au@NPFe$_2$O$_3$NC-modified GCE, suggesting the electrocatalytic redox reactions of ReHex at the GCE/Au@NPFe$_2$O$_3$NC electrode occurred mainly through the diffusion-controlled process.[11] Notably, the curve of i_{pc} and i_{pa} versus $v^{1/2}$ for the GCE/Au@NPFe$_2$O$_3$NC electrode showed a steeper slope than that of the unmodified GCE, further verifying the catalytic activity of Au@NPFe$_2$O$_3$NC towards the redox reaction of RuHex (Fig. S5B, ESI†). We also found that the catalytic i_{pc} of RuHex at the GCE/Au@NPFe$_2$O$_3$NC electrode increases with increasing RuHex concentration (Fig. S6, ESI†). To further understand the electrocatalytic activity, chronoamperometric (CA) responses were recorded at the GCE/Au@NPFe$_2$O$_3$NC electrode upon the successive addition of RuHex (Fig. S7, ESI†), where the CA response first increased steeply and then moved along the saturation. The calibration curve (Fig. S7B, ESI†) follows typical Michaelis-Menten equation for enzyme catalysis (details in the ESI†).[12] The apparent Michaelis-Menten constant (K_m^{app}) can be obtained from the electrochemical version of Lineweaver-Burk model (inset of Fig. S7B), and it was estimated to be 0.539 mM. This value is significantly low, suggesting the higher affinity of Au@NPFe$_2$O$_3$NC to RuHex, further verifying electrocatalytic activity of Au@NPFe$_2$O$_3$NC towards RuHex.[13] The electrocatalytic activity of this materials could be related to its smaller size, enhanced surface area, and superior electron transfer ability of porous Fe$_2$O$_3$ metal centre.[2,4]

We subsequently studied the [Ru(NH$_3$)$_6$]$^{3+/2+}$sytem using NPFe$_2$O$_3$NC before and after deposition of AuNPs into NPFe$_2$O$_3$NC. We found that 2% AuNPs loaded Au@NPFe$_2$O$_3$NC

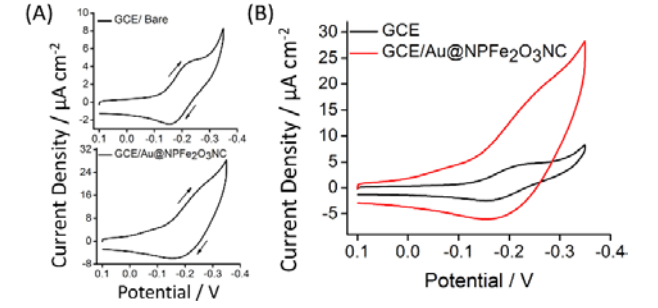

Fig. 2. (A) CVs obtained at an unmodified GCE (top) and Au@NPFe$_2$O$_3$NC-modified GCE (bottom) in 50μM RuHex (scan rate, 50 mVs^{-1}). (B) Comparison of these two

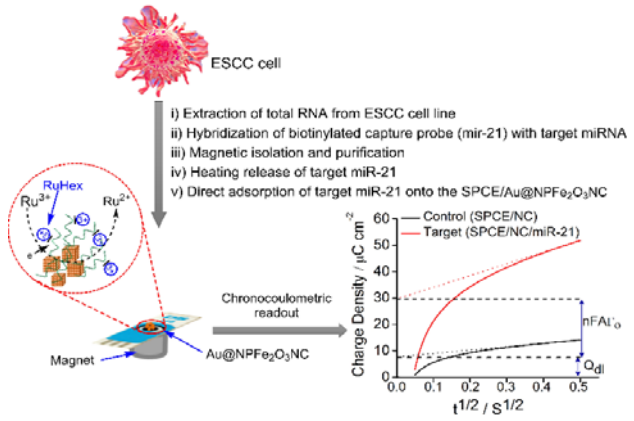

Fig. 3. Assay principle. miRNA was extracted from target cell lines or tissue samples. After magnetic isolation and purification, the target miR-21 was adsorbed onto the Au@NPFe$_2$O$_3$NC attached SPCE. An enhance electrochemical signals were generated by the CC interrogation of miRNA-bound $Ru(NH_3)_6]^{3+/2+}$ complexes. Inset, typical CC signals (charge density vs. $t^{1/2}$) showing the miRNA adsorbed SPCE/NC produces higher charge compare to an unmodified SPCE.

generated approximately 2-times lower i_{pc} in compare to that of NPFe$_2$O$_3$NC (20.11 vs 39.82 μAcm^{-2}, Fig. S8, ESI†). This findings suggest that deposition of AuNPs may reduce the surface dependent mass transport as well as nanocube mediated electron transfer, and hence reduces the resultant i_{pc}.[4,14] As our assay design requires the gold-DNA affinity interaction for adsorbing target miRNA, we synthesised porous Fe_2O_3 which favors the loading of AuNPs to achieve Au@NPFe$_2$O$_3$NC as a proof-of-concept particle framework.

The electrocatalytic activity of the Au@NPFe$_2$O$_3$NC can be used as a signal amplifying label for the detection of miR-21, a potential biomarker for detecting cancer in patients with oesophageal squamous cell carcinoma (ESSC).[15-17] miR-21 is usually upregulated in tissues, plasma or serum samples from patients with ESCC and significantly linked with poor OS (overall survival) in patients with ESCC.[18] Fig. 3 represents the outline of our assay. We initially extracted the total RNA from the tissue samples of ESCC using a commercial extraction kit. To capture specific miR-21 RNA present in this sample, we designed a biotinylated-capture probe and incubated it with the extracted sample. The target miRNA was hybridized with the biotinylated probe. The hybridized dsRNA was then magnetically separated and purified by streptavidin-modified dynabead based protocol. The captured miRNAs were heat released, separated and purified by another magnetic separation step (see ESI†). The isolated and purified miRNA were directly adsorbed onto the Au@NPFe$_2$O$_3$NC-modified screen-printed carbon electrode (SPCE/Au@NPFe$_2$O$_3$NC) *via* RNA-gold affinity interaction, which follows conventional physisorption and chemisorption mechanism. This involves the direct interaction of nitrogen atoms of nucleobase ring's with gold and partial contribution from the exocyclic amino group and charge transfer between the aromatic ring and gold surface.[19] The adsorbed miR-21 were then detected by the chronocoulometric (CC) charge interrogation in the presence of $[Ru(NH_3)_6]^{3+}$, which act as a signalling molecule that stoichiometrically binds to the anionic phosphate backbone of miRNA, and indicates the amount of miRNA adsorbed on the electrode surface.[10]

To check the assay functionality and specificity, we performed our assay with the same amount of starting synthetic miRNA (10nM) using Au@NPFe$_2$O$_3$NC-modified and unmodified-SPCE (Fig. 4A). As expected, the charge density (4.5 μCcm^{-2}) for the miR-21-attached (without Au@NPFe$_2$O$_3$NC) SPCE (*i.e.*, SPCE/miR-21) was very similar to that of the bare (without Au@NPFe$_2$O$_3$NC and miR-21) SPCE (i.e., SPCE/bare). A slightly higher response (4.5 versus 8.5 μCcm^{-2}) was estimated for the Au@NPFe$_2$O$_3$NC-modified SPCE (i.e., SPCE/NC/buffer, NOT), indicating a low level of adsorption of RuHex onto the surface of the SPCE/NC electrode. To evaluate the specificity of the capture probes for isolating miR-21 targets, we have also performed our assay using a noncomplementary miR-107 (i.e., SPCE/NC/miR-107) and compared the data against target miR-21 at the same starting concentration. We found that charges from experiments involving miR-107 were similar to the SPCE/NC electrode, indicating that our assay is not affected by the isolation of nonspecific RNAs present in the sample. Most importantly, the CC signal from the detection of target miR-21 was about 4-fold higher (8.79 vs 29.51 μCcm^{-2}) than that of the nonspecific miR-107. These experiments demonstrated the good specificity of our assay in isolating miR-21 RNA for miRNA-gold adsorption and subsequent electrocatalytic detection.

To evaluate the assay sensitivity, We tested designated concentration of synthetic target miR-21 ranging from 100 fM to 1.0 μM (Fig. 4B,C). The increasing level of Q_{RNA} was noted with increasing concentration of miRNA. This is attributed to the

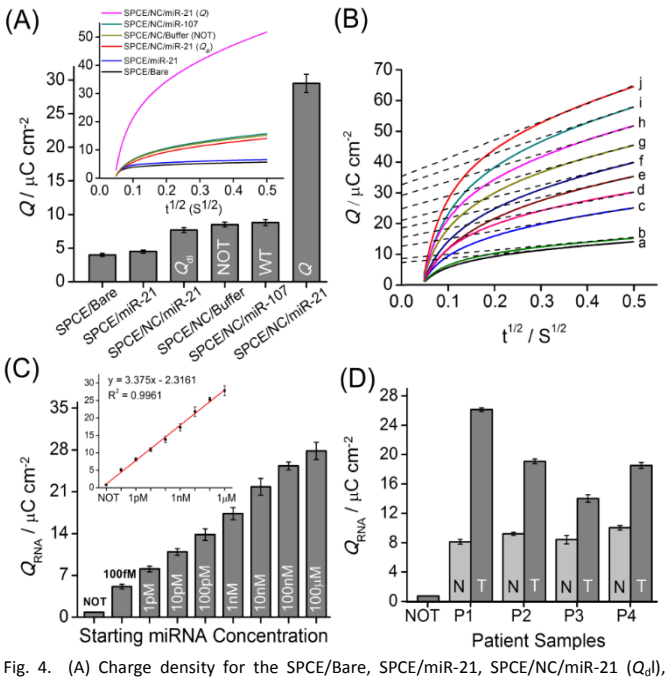

Fig. 4. (A) Charge density for the SPCE/Bare, SPCE/miR-21, SPCE/NC/miR-21 (Q_{dl}), SPCE/NC/buffer (NoT), SPCE/NC/miR-107 (Wrong target) and SPCE/NC/miR-21 (Q) electrodes. Concentration of miR-21 and miR-107 were 10 nM. (B) Typical CC curves for the (c-j) 100 fM-1.0 μM of synthetic miRNA. Curves a, and b are for the Q_{dl} and NOT respectively. (C) Charge density-concentration profiles. Inset, corresponding calibration plot. (D) Charge density obtained for eight tissue samples derived from ESCC patients. The concentration of RuHex is 50 μM. Each data point represents the average of three independent trails, and error bars represent the standard deviation of measurements (%RSD = <5%, for n = 3).

increased amount of miR-21, which was isolated and thus adsorbed onto the SPCE/ Au@NPFe$_2$O$_3$NC surface (the surface density were estimated to be 8.52 × 10^{13} and 1.60 × 10^{13} molecules/cm^2 for 1.0 μM and 100 fM of miR-21 respectively (see ESI† for details). An increased amount of adsorbed miR-21 bind with increased amount of $[Ru(NH_3)_6]^{3+}$ and thereby generating a higher Q_{RNA}. The linear regression equation was estimated to be y (charge density, μCcm^{-2}) = 3.375 (amount of miR-21) – 2.31, with a correlation coefficient (R^2) of 0.9961. The level of generated Q_{RNA} indicates that the minimum detectable miR-21 concentration is 100fM. The high sensitivity of the assay can be related to; (*i*) the large exposed surface area of AuNPs within the Au@NPFe$_2$O$_3$NC adsorbs more miRNA through the RNA-gold affinity interaction, thus larger amount of $[Ru(NH_3)_6]^{3+}$ ions bind on the miRNA-confined surface and (*ii*) electrocatalytic signal enhancement of $[Ru(NH_3)_6]^{3+/2+}$ system by Au@NPFe$_2$O$_3$NC.

The sensitivity of our method is similar or slightly better than those reported in previous methods[20-25](Table S1, ESI†). However, it is important to note that our method simplifies the assay design by avoiding the complex chemistries underlying each step of the sensor fabrication (i.e., cleaning of the electrode surface, formation of self-assembled monolayer, hybridization of the target with electrode-attached probe). Our assay also offer other advantages, such as (*i*) enhancement of the detection sensitivity through catalytic activity of porous framework of Au@NPFe$_2$O$_3$NC (*ii*) provides a mean for efficient removal of non-specific species and improves the isolation purity and efficiency using repetitive magnetic bead-based isolation and purification steps, (*iii*) disposable SPCE based electrochemical detection offer the high translational potential of the assay at relatively low cost (AUD$4 per electrode).

After establishing the sensitivity and specificity of the assay, we have performed clinical validation of the assay by analysing miR-21 levels in patient derived human ESCC cell lines, HKESC-1 and HKESC-4.[26] As shown in Fig. S9 (ESI†), with starting total RNA concentration of 10ng/mL, miR-21 levels were expressed at varying levels in these two cell lines. The expression of miR-21 in HKCSE-4 cells was found to be higher compared to HKCSE-1 cells (RT-qPCR validation data supported this results, see Fig S10A in ESI†). We further challenged our assay in-vivo by profiling the miR-21 expression in cancer and matched non-cancer tissue samples from patients diagnosed with ESSC. The ESSC patients (n=4) with primary tumours (denoted as T) and the adjacent non-neoplastic mucosae (denoted as N) from the same patients (matched) were used to detect miR-21 expression levels. Similar to cell lines, all paired cancer and non-cancer tissue samples from these patients showed varied levels of miR-21 expression. With the same amount of total RNA, our assay successfully detected a high expression of miR-21 in all four patients with ESCC (P1(T), P2(T), P3(T) and P4)(T) compared to their non-neoplastic counterparts (P1(N), P2 (N), P3 (N) and P4(N). High expression of miR-21 reported to have oncogenic effects in ESCC cells leading to increased cell proliferation and growth properties. Importantly, the conventional RT-qPCR study supported these data, and has noted approximately 3.0-, 1.5-, and 1.5-fold higher miR-21 expression in P1, P2 and P4 samples (Fig S10B in ESI†). The overexpression of miR-21 noted in this study are in agreement with previous findings on miR-21 expression.[15,17] Moreover, %RSD for n = 3, in quantifying the level of miR-21 in these clinical samples was found to be <5%. These data clearly indicated that CC signals generated by our assay were able to quantify the different degree of miR-21 level in ESCC tissue samples. Thus the method has potential implications for tracking the growth and progression of ESCC.

In conclusion, we have demonstrated the electrocatalytic activity of Au@NPFe$_2$O$_3$NC to develop an entirely new and sensitive electrochemical assay for non-enzymatic and amplification-free detection of miRNA. The applicability of our assay has been successfully tested and validated in cancer cell lines and a small cohort of tissue samples of patients with ESCC. We envisage that our method is not limited to miRNA detection, it could be further applied to detect a wide variety of RNA based biomarkers for other human cancers and chronic diseases.

This work was supported by the NHMRC CDF (APP1088966) to M.J.A.S.; HDR scholarships to M.K.M and M.N.I from University of Wollongong and Griffith University, respectively.

Notes and references

1 J. S. Beveridge*, et al.*, *Annu. Rev. Anal. Chem.,* 2011, **4**, 251-273.
2 V. Urbanova, M. Magro, *et al.*, *Chem. Mater.,* 2014, **26**, 6653-6673.
3 M. B. Zakaria, M. Hu, *et al*., *Eur. J. Inorg. Chem.*, 2014, **7**, 1137-1141; M. B. Zakaria, A. A. Belik, *et al*., *Chem. Asian J.* 2015, **10,** 1457.
4 K. C. Leung, S. Xuan, *et al*., *Chem. Soc. Rev.*, 2012, **41,** 1911-1928.
5 Y. Zhuo, P.X. Yuan, *et al.*, *Biomaterials,* 2009, **30**, 2284-2290; J. Zhao, Y. Zhang, *et al.*, *Biosens. Bioelectron.,* 2011, **26,** 2297-2303; B. Liu, Y. Cui, *et al.*, *Chem. Commun.,* 2012, **48,** 2624-2626.
6 H. Dong, J. Lei, *et al.*, *Chem. Rev.,* 2013, **113**, 6207-6233; S. Lin, and R. I. Gregory *Nat. Rev. Cancer*, 2015, **15**, 321-333.
7 É. Várallyay, J. Burgyán, *et al.*, *Nat. Protoc.,* 2008, **3**, 190-196; C. Chen, D. A. Ridzon, A. J. Broomer, *et. al.*, *Nucleic Acids Res.,* 2005, **33**, e179-e179.
8 E. A. Lusi, M. Passamano, *et al*., *Anal. Chem.,* 2009, **81**, 2819-2822; X. Wu, Y. Chai, *et al*., *ACS Appl. Mater. Interfaces*, 2014, 7, 713-720; N. Xia, X. J. Wang, *et al., Int. J. Electrochem. Sc.,* 2013, **8**, 9714-9722.
9 E. Hamidi-Asl, I. Palchetti, *et al.*, *Talanta*, 2013, **115**, 74-83.
10 J. Zhang, S. Song, L. Zhang, *et al*., *J. Am. Chem. Soc.,* 2006, **128**, 8575-8580.
11 A.J. Bard, and L. R. Faulkner, *Electrochemical Methods*, John Wiley & Sons, New York, 1980, 199-206.
12 A. L. Lehninger, D. L. Nelson, and M. M. Cox, *Lehninger Principles of Biochemistry*, W.H.Freeman & Co Ltd, New York, 2005.
13 H. Lineweaver and D. Burk, *J. Am. Chem. Soc.* 1934, **56**, 658-666; A. K. Dutta *et al., J. Mol. Catal. A Chem.*, 2012, **360**, 71-77.
14 H. Z. Cui, et al.,Y. Guo, X. Wang, C. J. Jia and R. Si, *Catalysts*, 2016, **6**, 37.
15 M. Winther, J. Alsner, *et al.*, *Acta Oncologica*, 2015, **54**, 1582-1591.
16 Y. Mori, H. Ishiguro, Y. Kuwabara, *et al.*, *Mol. Med. Rep.*, 2009, **2**, 235-239; Y. Tanaka, H. Kamohara, K. Kinoshita, *et. al.*, *Cancer*, 2013, **119**, 1159-1167.
17 N. Nouraee, K. Van Roosbroeck, M. Vasei, *et al.*, *Plos One*, 2013 **8,** e73009; S. Komatsu, D. Ichikawa, T. Kawaguchi, *et al., Am. J. Cancer Res.,* 2016, **6**, 1511.
18 R. Kumarswamy, I. Volkmann, and T. Thum *RNA Biol.*. 2011, **8**, 706–713.
19 K. M. Koo, A. A. Sina, *et al*., *Anal. Methods,* 2015, **7,** 7042-7054; A. A.I. Sina, S. Howell, et al., *Chem. Commun.*, 2014, **50**, 13153-13156.
20 H. Cao, S. Liu, *et. al*., *Chem. Commun.*, 2014, **50**, 13315-13318.
21 G. J. Zhang, J. H. Chua, *et al*., *Biosens. Bioelectron.*, 2009, **24**, 2504-2508.
22 K. M. Koo, L. G. Carrascosa, *et al*., *Anal. Chem.*, 2016, **88**, 2000-2005.
23 B. Yao, Y. Liu*, et al*., *Chem. Commun.*, 2014, **50**, 9704-9706.
24 M. Bartosik, M. Trefulka, *et al.*, *Electrochem. Commun.,* 2013, **33**, 55-58.
25 Y. Wen, G. Liu, *et al.*, *Methods*, 2013, **64,** 276-282.
26 Y. C. Hu, *et al.*, *Cancer Genet. Cytogenet.,* 2000, **118**,112-120; L. C. Cheung, Cancer Genet. Cytogenet., 2007,**178**, 17-25.

